Bay sedimentation as controlled by regional crustal behaviour, local tectonics and eustatic sea-level changes: Coquimbo Formation (Miocene–Pliocene), Bay of Tongoy, central Chile

J.P. Le Roux [a,*], Danisa M. Olivares [a], Sven N. Nielsen [b], Norman D. Smith [c], Heather Middleton [d], Juliane Fenner [e], Scott E. Ishman [f]

[a] *Departamento de Geología, Facultad de Ciencias Físicas y Matemáticas, Universidad de Chile, Casilla 13518, Correo 21, Santiago, Chile*
[b] *GeoForschungsZentrum Potsdam, Section 3.1, Telegrafenberg, 14473 Potsdam, Germany*
[c] *Department of Geosciences, University of Nebraska, Lincoln, Nebraska 6588-0340, USA*
[d] *CSIRO Petroleum, Riverside Corporate Park, Delhi Road, North Ryde, NSW 2113, Australia*
[e] *Section Marine Geology, Federal Institute for Geological Research and Resources, Stilleweg 2, D 30655 Hannover, Germany*
[f] *Department of Geology, Southern Illinois University, Carbondale, IL 62901-4324, USA*

Abstract

The north-facing Bay of Tongoy in central Chile is flanked by topographic highs in the west and east. During the Miocene and Pliocene, the bay extended inland at least 30 km farther south than a present. It was filled with muds, sands, coquinas and gravel during a series of transgressions and regressions related to regional and local tectonic movements combined with global sea-level variations. $^{87}Sr/^{86}Sr$ and microfossil dating indicates transgressions between 11.9–11.2 Ma, 10.1–9.5 Ma, 9.0–7.3 Ma, 6.3–5.3 Ma, 4.3–2.2 Ma and 1.7–1.4 Ma. The regional tectonic behaviour of the crust shows general uplifting from 10.5 Ma to 6.9 Ma, associated with subduction of the Juan Fernández Ridge (JFR) beneath this part of the continent. Subsidence followed between 6.9 and 2.1 Ma, in the wake of the southeastward-migrating JFR. The subsequent subduction of an oceanic plateau similar to the JFR caused rapid uplift that led to the final emergence of the bay above sea level. The Puerto Aldea normal fault along the western limit of the study area was reactivated during the regional uplift and subsidence events, with reverse faulting occurring during the latter phase. Sporadic fault reactivation probably triggered the rapid changes in water depth reflected in the recorded vertical succession of facies.

Keywords: Bay sedimentation; Juan Fernández Ridge; Geohistory analysis; Miocene; Pliocene; Chile

1. Introduction

Bays are complex depositional environments because they are not only affected by input from rivers but also by wave action and marine currents. Sediments are therefore dispersed in different directions, often mixing with deposits derived from other areas or transported by different processes. Furthermore, relative sea level oscillations caused by eustatic changes as well as regional and local tectonics can cause abrupt changes in water depths. Rapid lateral and vertical facies changes are therefore typical of bay deposits.

* Corresponding author.
E-mail address: jroux@ing.uchile.cl (J.P. Le Roux).

At Tongoy 57 km south of La Serena, central Chile (Fig. 1), Miocene–Pliocene sandstones, shales, conglomerates and coquinas, belonging to the Coquimbo Formation, were interpreted as shallow marine or bay-fill sediments by López (1965), Paskoff (1970), Martınez (1979), and Martınez and Caro (1980), but without a detailed description or analysis of facies. In an attempt to understand this complex succession of greatly varied sediment types and contained faunal assemblages within the context of relative sea level changes in a tectonically active setting, we followed a multidisciplinary approach including facies and geohistory analysis, macro- and microfossil studies, and $^{87}Sr/^{86}Sr$ dating.

2. Geological background

2.1. Tectonic and structural framework

The Coquimbo Formation forms part of a discontinuous series of Late Cretaceous to Neogene basins (Fig. 1) extending along the Chilean coastline from Antofagasta (23°S) to the Taitao Peninsula (47°S). All of these basins have been affected by subduction of the Nazca and Antarctic oceanic plates beneath the South American continent, which profoundly affected sea level changes and sedimentary processes (e.g. Le Roux and Elgueta, 2000; Le Roux et al., 2004, 2005a,b). Within the Chilean flat-slab sector between 26°S and 33°S (Pardo et al., 2002) the subduction of oceanic plateaux such as the Juan Fernández Ridge (JFR), has played a particularly prominent role. Le Roux et al. (2005a,b), in a study at Carrizalillo about 150 km north of Tongoy (Fig. 1), concluded that uplift of around 80 m was caused by the subduction of the JFR beneath this part of the continent, followed by subsidence of about 140 m as the ridge migrated southeastward along the coastline (Yáñez et al., 2002). It is therefore to be expected that the JFR would have had a similar effect on sea level changes in the Tongoy area.

Herm et al. (1967) and Herm (1969) considered the paleobay to have developed within a tectonic graben structure, whereas Paskoff (1970) proposed a half-graben for a lack of clear evidence for faulting along its eastern limit. During a detailed structural analysis of the area, Heinze (2003) also failed to find any evidence for large-scale faulting at the eastern boundary. At the western boundary, however, the N- to S-oriented Puerto Aldea Fault has a normal displacement to the east (Paskoff, 1970; Martínez, 1979), bringing the Coquimbo Formation in contact with Triassic–Jurassic intrusives (Fig. 2). Geophysical data (Herm et al., 1967)

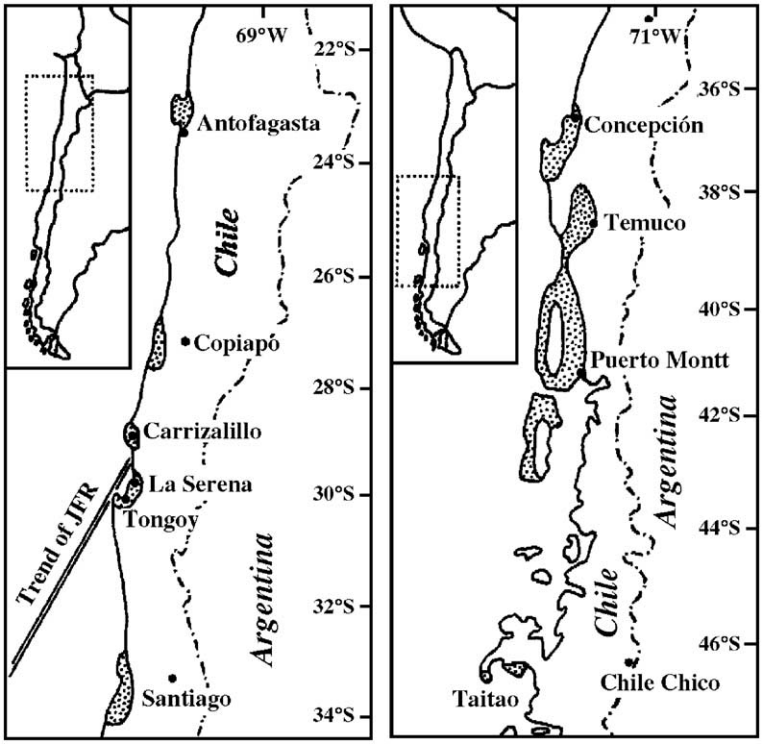

Fig. 1. Distribution of Neogene basins along the Chilean coastline. Position of Juan Fernández Ridge shown at ca. 7 Ma.

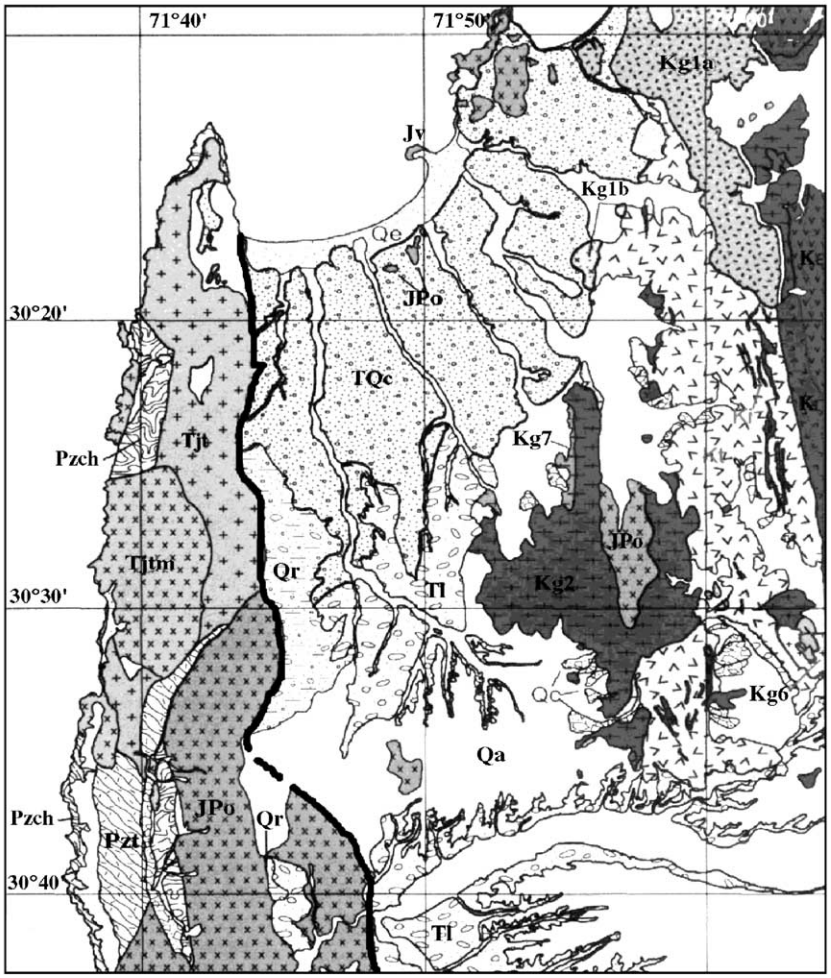

Fig. 2. Geological map of the Tongoy area (modified from Gana, 1991). Qa: Alluvial deposits; Qe: Aeolian deposits; Qc: Colluvial deposits; Qr: Regolith; TQc: Coquimbo Formation; Tl: Limarı Formation; Ka: Arqueros Formation; Kt: Tamaya Beds; Kr: El Reloj Beds; Jv: Algarrobal Formation; Tjt: Talinay Unit; Tjtm: Tranquilla–Millahue Unit; Jpo: Puerto Oscuro Unit; Kg1a, Kg1b, Kg2, Kg6, Kg7: Lower Cretaceous granitoids; Ki: Intrusive riolites; Pzch: Choapa Metamorphic Complex; Pzt: Talquilla gneiss. Heavy black line is Puerto Aldea Fault.

suggest that the basement within the half-graben lies at a depth of between 100 and 360 m along Quebrada Pachingo (Fig. 3), deepening towards the north. Other, less prominent normal faults in the area are generally oriented N–S, whereas dextral strike–slip faults have a NE–SW orientation (Benado, 2000). Heinze (2003) also identified numerous short, trench-parallel faults rupturing the Plio-Pleistocene sedimentary cover, indicating that tectonic movements continued after deposition of the Coquimbo Formation.

2.2. Geomorphology and paleogeomorphology

The present Bay of Tongoy is flanked by two prominent, north-striking geomorphologic features (Fig. 3). West of the Puerto Aldea Fault lies a rocky ridge (Altos de Talinay) consisting of Paleozoic basement rocks and Mesozoic felsic intrusives. A prominent hill (Cerro Guanaquero) consisting of Mesozoic gabbros and quartzose monzodiorites lies to the east. Cerro Guanaquero probably formed an island within a larger paleobay that included the present Bay of Guanaquero and was flanked further east by a mountain belt extending southward to the Limarí River (Fig. 3). Between this mountainous area and Altos de Talinay lies a central lowland covering approximately 100 km^2, traversed by NNW-trending dry valleys or “quebradas” named Pachingo, Salinas (Los Litres), Los Almendros, Tongoy (Los Camarones) and El Romeral, from west to east (Fig. 3). Southwards the lowland rises gently to a

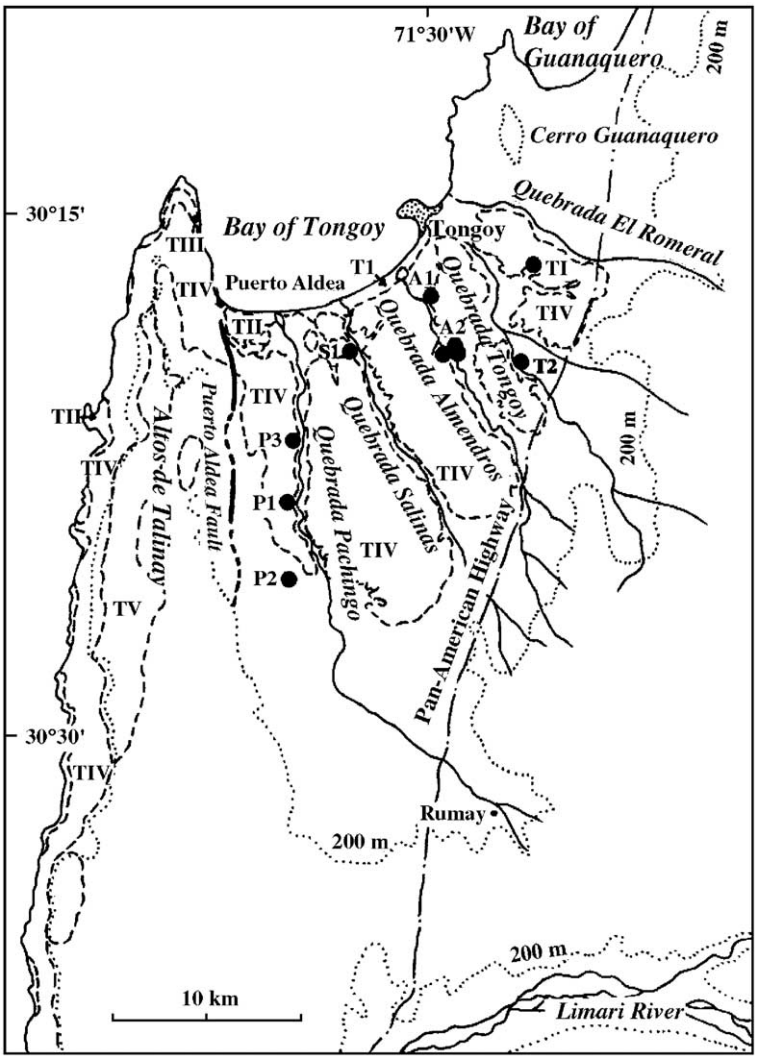

Fig. 3. Physiography and geomorphology of the Tongoy area showing location of measured stratigraphic columns (T1, T2: Tongoy 1, 2; A1, A2: Almendros 1, 2; S1: Salinas 1; P1, P2, P3: Pachingo 1, 2, 3) and marine terraces (TI, TII, TIII, TIV, TV: Talinay I, II, III, IV, V).

maximum elevation of about 340 m before descending to the EW-trending valley of the Limarí River at less than 150 m a.s.l. The central lowland is underlain by the Miocene–Pliocene Coquimbo Formation, which was affected by four distinct episodes of marine transgression and regression during the Holocene (Benado, 2000), leaving wave-cut terraces known as Talinay I–IV from youngest to oldest, respectively (Fig. 3).

A possible scenario for a Mio-Pliocene depositional environment in this area is a single large estuary flanked by the Altos de Talinay and eastern highlands. Estuaries are defined as sites of "constant interaction between. . .freshwater river and marine tidal currents and waves" (Leeder, 1999) and represent ". . .the seaward termination of a single river channel. . ." (Dalrymple et al., 1992). However, according to this definition, that environment seems unlikely. Present-day perennial rivers, which are mainly supplied by melting snow in the Andes and have very limited discharges, all flow to the west or southwest, including the Limarí River at the southern boundary of the study area. Although Brüggen (1950) and Herm (1969) maintained that the Limarí River originally flowed into the Bay of Tongoy, they did not offer any supporting evidence. Moreover, the Limarí River cuts almost straight through the southward extension of Altos de Talinay. This implies incised drainage, and begs the question why it should have deviated west to traverse the hard, intrusive basement rocks if it originally crossed the poorly consolidated deposits of the Coquimbo deposits to the north, which

would have been much easier to erode. Furthermore, sandstones in the Coquimbo Formation are also arkosic, containing on average 50–60% quartz and 30–40% feldspar, with subrounded to subangular grains (López, 1965), suggesting a relatively short distance of transport. Their source areas are probably the felsic intrusives surrounding the study area and not the andesitic volcanics of the Andes, where the Limarí River originates.

There is strong evidence that climatic conditions during deposition of the Coquimbo Formation were as arid as today when the north-trending quebradas flow strongly only after rare severe rainstorms in the interior. Alpers and Brimhall (1988), using geochronologic dating and paleotopographic reconstruction, estimated average erosion rates during different phases of mineralization in the Atacama Desert and concluded that hyperarid conditions were established there ca. 15 Ma. This may be related to a major global cooling between 15 and 12.5 Ma (Flower and Kennett, 1993; Wright, 1998), as well as the intensification of coastal upwelling in the eastern Pacific around 14–11 Ma (Dunbar et al., 1990; Tsuchi, 1997). These factors would have caused a general aridification of the Atacama region (Gregory-Wodzicki, 2000) and its adjoining areas. In central Chile, this is supported by paleobotanical evidence, which also indicates that aridification commenced in the middle Miocene at around 15 Ma (Hinojosa and Villagrán, 1997; Hinojosa, 2005). It therefore seems unlikely that any major perennial river could have drained into the Bay of Tongoy to create large-scale estuarine conditions. Even if the Limarí River did flow northwards during the Miocene–Pliocene, its low-volume run-off would have had only a limited effect within the much larger confines of the bay.

The southern boundary of the bay during Miocene times is marked by aeolian dune deposits just east of the Pan-American Highway near Rumay (Fig. 3), where cream to reddish, fine to medium sandstones show large-scale cross-lamination dipping in different directions. Cross-bed sets are more than 2 m thick and individual foresets reach more than 5 m in length. Along the Pan-American Highway in the vicinity of Quebrada El Romeral (Fig. 3), a succession of reddish brown to buff, intensely bioturbated mudstones are cut by small channels containing gravel at the base, that fines upward into medium and fine sandstone (Fig. 4). Thin, nodular limestone horizons are also present. This succession probably represents a tidal flat environment traversed by tidal creeks, indicating the eastern limit of marine influence.

3. Stratigraphy

Herm (1969) studied the sedimentary succession along Quebrada Pachingo and differentiated 14 units that he identified as Pliocene and early Pleistocene, truncated by middle Pleistocene terraces associated with a transgressive cycle. He also distinguished a second late Pleistocene transgression. The latter was correlated with the Cachagua stage (Herm and Paskoff,

Fig. 4. Tidal creek within tidal flat deposits along the Pan-American Highway. Security fence along road is about 1 m high.

1967) and the younger sediments were thought to be part of a Holocene transgression–regression sequence (Vega Stage) consisting of several beach ridges with fauna similar to the modern berm.

We measured 16 stratigraphic sections along four of the five quebradas (Fig. 3), with additional information obtained from road cuts throughout the study area. Of the measured sections, the stratigraphically most complete is Pachingo 3 (Fig. 5) that it is used as the reference profile. At this locality, the succession can be divided into 16 different units (Table 1) that can be correlated throughout most of the study area. These units represent not only different stratigraphic levels, but also distinct facies associations that can be interpreted in terms of specific depositional environments.

The measured section of Herm (1969, Fig. 32) agrees fairly well with our data; however, incorporation of ages from a study of a nearby section by Tsuchi et al. (1988, 1990) is difficult because their published column resembles neither ours nor that of Herm (1969).

4. Dating the stratigraphic units

Dating by $^{87}Sr/^{86}Sr$ isotopes was performed with a VG354 thermal ionisation mass spectrometer at the CSIRO in North Ryde, Australia, using mainly macrofossil shells. The analytical procedures are described in Le Roux et al. (2005b). The precision of the McArthur et al. (2001) curve used for dating varies between about 0.4 Ma and 0.1 Ma for the middle Miocene to Pliocene, but with analytical errors the total error could be up to ± 1.2 Ma.

Unit 1 contains *Turritella leptogramma*, which according to DeVries (in press), also occurs in late Miocene deposits in southern Peru. In Chile, this species has been reported from Navidad (Tavera, 1979) where an early Miocene age is possible (Finger et al., 2003; Nielsen et al., 2003). A Sr date of 11.9 ± 1.0 Ma for the overlying Unit 3, however, constrains the age of Unit 1 to between 23.0 and about 11 Ma.

For Unit 3, the Sr date of 11.9 ± 1.0 Ma (Serravalian) was obtained from an apparently in situ, uniden-

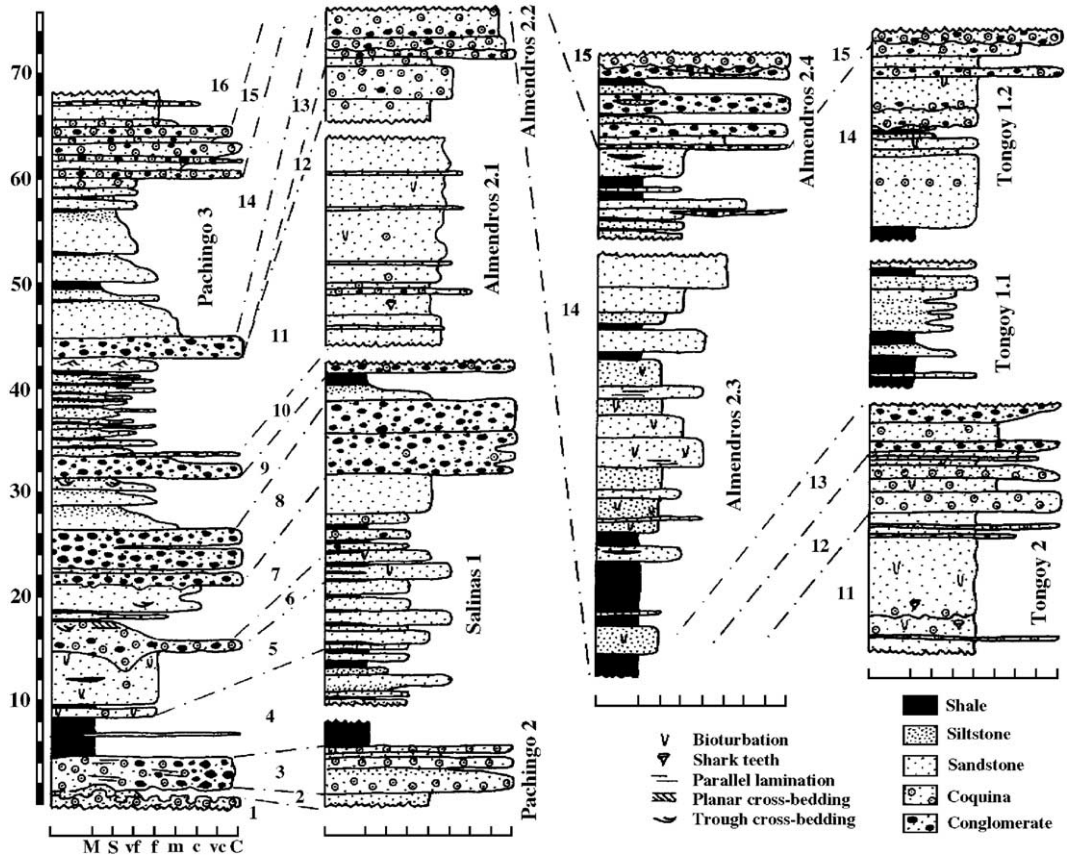

Fig. 5. Measured stratigraphic columns showing correlation between units. For location of columns, see Fig. 3.

Table 1
Lithostratigraphic units in the Coquimbo Formation

Unit	Facies	Macrofossils
16	Sandstone, limestone	*Balanus* sp.
15	Conglomerate, calcareous conglomerate, coquina, sandstone, siltstone, mudstone	*Acanthina unicornis*, *Turritella* sp., *Balanus* sp., gastropods, pelecypods
14	Sandstone, siltstone, shale, mudstone	*Turritella* sp., *Balanus* sp., *Ostrea* sp.
13	Conglomerate, coquina, sandstone	*Balanus* sp., *Ostrea* sp., gastropods, cetacean bones
12	Coquina, sandstone	*Chorus* sp., *Balanus* sp., *Ostrea* sp., bivalves, gastropods, cetacean bones
11	Sandstone, clay	*Chlamys hupeanus*, *Chorus* sp., *Ostrea* sp., *Balanus* sp., gastropods, *Carcharodon carcharias* teeth, cetacean bones, fish scales
10	Conglomerate, sandstone	*Turritella* sp., *Balanus* sp., gastropods, bivalves
9	Sandstone, siltstone, clay	
8	Conglomerate, sandstone, siltstone	*Ostrea* sp., *Balanus* sp., bivalves, gastropods
7	Sandstone, siltstone, shale, clay	Gastropods
6	Conglomerate, coquina, sandstone	*Ostrea* sp., *Chlamys* sp., *Crepidula* sp., *Balanus* sp., gastropods
5	Sandstone, diatomaceous clay, shale	
4	Tuffaceous and diatomaceous clay, siltstone, sandstone, phosphate pebble bed	Bivalves, gastropods, cetacean bones, fish scales, sponge spicules, *Cosmopolitodus hastalis* teeth
3	Coquina, conglomerate	*Turritella leptogramma*, *Mulinia* cf. *vidali*, *Chlamys* sp., *Balanus* sp. *Ostrea* sp., gastropods, cetacean bones
2	Brecciated sandstone	
1	Coquina	*Turritella leptogramma*, gastropods

tified shell collected about 5 m from the base of the Pachingo 2 column.

The presence of *Coscinodiscus plicatus* in Unit 4 at Pachingo 3 indicates an age ranging from 14.2 to 8.7 Ma. Martínez and Caro (1980) also recovered various microfossils from Unit 4 in the Salinas 1 section (Table 2). The diatoms *Actinocyclus ellipticus* (N9–N15) and *Rhaphoneis miocenica* (N13–N21) occur together with the ebridians *Ammodochium rectangulare* and *Ebriopsis antiqua*, both of which extend from the Paleogene into zone N15. The concurrent range between N13 and N15 thus indicates a Serravalian age, i.e. about 13.7 to 11.6 Ma according to the updated chart of the International Commission on Stratigraphy (2004). Tsuchi et al. (1988, 1990) also dated several units of the Pachingo section (called El Rincón by them) using planktonic foraminifers and diatoms. A basal shale bed, probably Unit 4, yielded the diatoms *Azpeitia nodulifer* (14.2–0 Ma), *Coscinodiscus plicatus* (14.2–8.6 Ma), *Denticulopsis hustedtii* (14.2–8.7 Ma), and *Synedra jouseana* (23–10.4 Ma), indicating an overlapping age range of 14.2 to 10.4 Ma for this bed. If an age of 11.9 Ma is

Table 2
Microfossils recorded in facies 6 by Martínez and Caro (1980) and present authors

Diatoms
Actinocyclus octonarius
Actinocyclus ellipticus
Actinoptychus senarius
Auliscus caelatus var. *constricta*
Azpeitia sp.
Biddulphia aurita
Cocconeis sp.
Coscinodiscus apiculatus ambiguus
Coscinodiscus asteromphalus
Coscinodiscus divisus
Coscinodiscus marginatus
Coscinodiscus neoradiatus
Coscinodiscus oculoiridis
Coscinodiscus perforatus
Coscinodiscus plicatus
Coscinodiscus radiatus borealis
Coscinodiscus radiatus parvus
Coscinodiscus subsalsus (?)
Cymbella sp.
Diploneis cabro
Diploneis pseudobombiformis
Grammatophora angulosa
Navicula lyra
Opephoropsis tiltilensis
Paralia coronata
Paralia sulcata
Plagiogramma obesum
Raphoneis miocenica
Raphoneis surirelloides
Stephanopyxis sp.
Symbolophora stellaris
Thalassiosira leptopus
Triceratium cinnamomeum
Ebridians
Ammodochium rectangulare
Ebriopsis antiqua
Dinoflagellates
Actiniscus pentasterias
Silicoflagellates
Distephanus speculum
Mesocena elliptica

accepted for Unit 3, Unit 4 therefore has a mean age close to 11.2 Ma. This is supported by the presence of *Cosmopolitodus hastalis* teeth in the phosphate bed, which according to Mario Suárez (personal communication, 2005) are common in similar phosphate beds of Tortonian to Messinian age west of Copiapó (Fig. 1).

From another shale bed about 1 m higher in their section, Tsuchi et al. (1988) reported the planktonic foraminifers *Globigerinoides sicanus*, *Praeorbulina glomerosa*, and *Globigerinatella insueta* and concluded a Langhian (N8b) age. However, this range of 16.0–13.7 Ma exceeds the ages of the units below and may indicate reworking of older sediments.

Several diatoms – *Denticulopsis hustedtii* (14.2–8.7 Ma), *Rhizosolenia miocenica* (?–8.2 Ma), *Stephanopyxis schenckii* (14.2–7.8 Ma), and *Coscinodiscus plicatus* (14.2–8.7 Ma) – were recovered from a shale bed (Tsuchi et al., 1990) possibly within Unit 7. The composite age is 14.2–8.7 Ma.

A Sr age of 9.0 ± 1.0 Ma was obtained from a shell fragment near the middle of Unit 8 in the Salinas 1 column. Accepting this age for Unit 8 and assuming a constant rate of sedimentation between Units 4 and 8, mean ages of 10.6, 10.1 and 9.5 Ma can be assumed for Units 5, 6 and 7, respectively. The latter age thus falls within the possible range given by diatoms in Unit 7.

A single specimen of the planktonic foraminifer *Orbulina universa* was reported by Tsuchi et al. (1988) for a sandstone bed possibly within Unit 9. They gave the age as N9, which corresponds to about 15 Ma. This age, together with that given for Unit 5 by Tsuchi et al. (1988), shows that ages derived from foraminifers and diatoms are not always consistent. The diatom ages, however, agree well with our Sr ages. The older foraminifer ages may indicate reworking of older sediments, as was demonstrated for other Miocene localities further south along the Chilean coast (Finger et al., 2003; Nielsen et al., 2003).

Unit 11 in Tongoy 2 contains teeth of the great white shark *Carcharodon carcharias* associated with cetacean bones. In the Pisco Formation of Peru, these teeth are used as a zone fossil for the Pliocene (De Muizón and DeVries, 1985). This species is also common in Pliocene deposits at La Herradura (Suárez and Marquardt, 2003) and Antofagasta (Suárez et al., 2003) further north. The presence of *Chlamys hupeanus* in this unit would indicate a late Pliocene age according to Herm (1969), but Guzmán et al. (2000) pointed out that Herm in general dated early Pliocene deposits as late Pliocene and late Miocene deposits as early Pliocene. If a Pliocene age is thus accepted for Unit 11, it has a probable range of 5.3 to 1.8 Ma. However, because a sample from the base of Unit 12 at Tongoy 2 was Sr dated at 5.2 ± 0.7 Ma, Unit 11 is assigned its maximum age of 5.3 Ma. Taking into account the stratigraphic thickness of Units 9 and 10 and again assuming a constant rate of sedimentation, mean ages close to 7.3 and 6.3 Ma can be respectively assigned to these two units.

Two Sr dates were obtained for Unit 12. As mentioned above, a sample from the base of the unit in Tongoy 2 yielded an age of 5.2 ± 0.7 Ma, whereas another sample taken about 2 m above the base in Almendros 2.2 gave an age of 4.9 ± 0.7 Ma. A mean age of 5.0 Ma is therefore assumed for Unit 12.

Unit 14 also yielded two Sr dates. In Tongoy 2, a sample taken about 6 m from the top was dated at 2.2 ± 0.5 Ma, compared to an age of 1.8 ± 0.5 Ma for a sample from the uppermost meter of the unit in Tongoy 1.2. Taking the age of Unit 14 about 3 m from its top to be 2.0 Ma and again assuming a constant rate of sedimentation, the age of Unit 13 would be about 4.3 Ma.

Unit 15 was Sr-dated at 1.4 ± 0.5 Ma. This is supported by the presence of *Acanthina unicornis* in this unit, which was shown by DeVries (2003) to have evolved from *Acanthina triangularis* between 3 and 2 Ma.

Extrapolating the same rate of sedimentation would give a mean age of 1.2 Ma for Unit 16.

5. Facies description and interpretation

The neritic environment can be divided into several zones (e.g. Nichols, 1999, Fig. 14.1). These are the foreshore or beach between high and low tide, the upper shoreface from the low tide level to the fair weather wave base, the lower shoreface between the fair weather and storm wave base, and the continental shelf or offshore area, generally below the storm wave base to the edge of the continental shelf. Because there is no general agreement in the literature on the absolute water depths of these zones, we used the following system: The depth to which waves disturb the ocean floor is half the wavelength, which depends on the velocity, fetch and duration of the wind. From equations and graphs representing the relationships among these variables (U.S. Army Corps of Engineers, 2002), the wavelength can be determined roughly from the wind velocity for a fully developed sea. For a 25-knot wind (46 km/h; a strong breeze according to the Universal Sea State Code or USSC), the average wavelength would be about 80 m, so that we consider 40 m to be the lower boundary of the upper shoreface. Si-

milarly, we consider the transitional zone (middle shoreface) to correspond to a wind velocity of between 25 and 30 knots (up to 55 km/h; a moderate gale according to the USSC), which would give rise to wavelengths of about 120 m, affecting the ocean floor to a depth of 60 m. Storms are considered to be represented by wind speeds exceeding 30 knots (gales to storms according to the USSC) and can affect the whole shelf. Because the continental shelf is generally considered to lie at a depth of 100–200 m, we take 100 m to be the cut-off between the outer shoreface and inner shelf or bay. The following water depths are therefore considered to be representative of the different sedimentary environments (average depth in brackets): foreshore/littoral zone = 0 m; estuary = 5–15 m (10 m); upper shoreface = 0–40 m (20 m); middle shoreface = 40–60 m (50 m); lower shoreface = 60–100 m (80 m); inner shelf/bay = 100–140 m (120 m).

5.1. Facies 1: terra rossa and sandstone breccia

5.1.1. Description

This facies, only observed in Unit 2, consists of buff to orange brown, poorly sorted, clay-rich sandstone filling fissures and cavities within coquina. The sandstone is brecciated within some of the cavities (Fig. 6).

5.1.2. Interpretation

Subaerial dissolution of the calcareous matrix of the coquina released fine sand particles, forming a soil profile of "terra rossa" (Esteban and Klappa, 1983). Partial consolidation of the soil evidently occurred before some of the underground cavities collapsed, forming the sandstone breccia. This facies therefore represents a subaerial, probably coastal plain environment.

5.2. Facies 2: clast- and matrix-supported conglomerates interbedded with pebbly sandstone, coarse to medium sandstone and occasional mudrocks

5.2.1. Description

Facies 2 occurs in Units 8, 10 and 13 where it always shows sharp to erosional basal contacts. It consists of poorly consolidated clast- and matrix-supported conglomerates with well-rounded, fair to well-sorted pebbles and cobbles of andesite and sandstone, normally less than 10 cm but up to about 25 cm in diameter, in a medium to coarse sandy matrix. The clasts constitute 50% to 80% of the rock. In some cases (e.g. Pachingo 1), there is no clear imbrication, but at Salinas 1 pebbles are distinctly inclined southwards. The conglomerate units vary between 100 and 150 cm in thickness, with internal stratification produced by pebble size and sorting.

The conglomerates are interbedded with brownish grey sandstones containing up to 10% pebbles and fragments of *Balanus*, *Ostrea* and *Turritella*, as well as other gastropods, bivalves and occasional cetacean bones. In some areas, they are also interbedded with grey to purplish brown, well-cemented, medium to coarse sandstone lenses and beds up to about 2 m thick. The sandstones are generally massive, but show occasional upper flow regime planar lamination. In the Almendros 2.4 section, matrix- and clast-supported conglomerates are overlain by fining-upward succes-

Fig. 6. Karst development within coquina, showing sedimentary breccia of the overlying "terra rossa" (facies 2) that collapsed into small sinkholes (Pachingo 3).

sions of sandstone, ochre-weathering siltstone and mudstone.

In Tongoy 2, subangular to subrounded megaclasts reaching more than 1 m in diameter occur at the top of coarsening-upward matrix-supported conglomerates abruptly overlain by fine sandstones (Fig. 7).

5.2.2. Interpretation

The presence of thick-shelled shallow marine fossils including *Ostrea* and *Balanus*, as well as cetacean bones within this facies, indicates an upper shoreface environment (Bourgeois and Leithold, 1984). According to MacEachern and Hobbs (2004), conglomerates and conglomeratic sandstones of open bays are largely confined to the bay margins, whereas Nemec and Steel (1984) confirm the tendency for gravel to be trapped in or near river mouths. It may therefore be difficult to distinguish such marine deposits from closely associated fluvial deposits. However, upper shoreface conglomerates are generally more sheet-like than fluvial conglomerates because of storm-wave reworking (Kumar and Sanders, 1976). Clifton (1973) also concluded that wave-reworked gravels are laterally more continuous than alluvial gravel and that pebbles are better segregated into discrete beds. Similarly, MacEachern and Hobbs (2004) described well-sorted, clast-supported conglomerates displaying good clast segregation, interbedded with sandstones and pebbly sandstones, from an upper shoreface environment in Alberta and British Columbia. The crude stratification, pebble sorting and sandstone interbeds of facies 2 are consistent with these observations and probably reflect changing energy conditions between storms and fair weather periods.

The local imbrication developed within this conglomerate indicates deposition by strong unidirectional currents entering the bay from the south, parallel to the present quebradas. A relatively high-energy environment is also supported by the upper flow regime planar lamination of the interbedded sandstones. The latter probably reflect waning runoff and storm conditions, as confirmed by the local presence of fining-upward successions.

The presence of protruding megaclasts at the top of unimbricated, coarsening-upward, matrix-supported conglomerates in some areas suggests that gravity flow processes occurred from time to time (Sohn, 2000; Le Roux et al., 2004). Arnott (2003) also attributed planar-based matrix-supported conglomerate abruptly overlain by pebbly and very coarse sandstone in the Cardium Formation of Alberta as having been deposited from high-concentration gravity-flow dispersions. In the Tongoy paleobay, similar mechanisms probably operated after extreme discharge periods. In a semi-arid environment, the scarcity of vegetation results in rivers acquiring a very high suspended load during such events, producing dense slurries capable of transporting very large clasts. The presence of dune sands around the southern shoreline of the Tongoy paleobay would have favoured the development of such dense sediment–water mixtures.

Fig. 7. Megaclast within coarsening-upward matrix-supported conglomerate, facies 2 (Tongoy 2). Hammer (in rectangle) for scale.

Facies 2 is therefore considered to represent fluvio-estuarine conditions near local river mouths where coarse gravels and pebbly sands were deposited during periods of intense runoff. During the waning stages of storms or continental runoff events, fining-upward successions of sand and locally mud accumulated. It is also possible that some sandy interbeds resulted from wave action winnowing previously deposited, matrix-supported gravels during storms, thereafter redepositing the finer fraction on top of the latter during the return to normal weather conditions.

5.3. Facies 3: coquina with interbedded medium to very fine sandstones

5.3.1. Description

Facies 3 occurs in Units 1, 3, 6, 8, 12, 13 and 15. It consists of generally lenticular, up to 2-m-thick units overlying sharp to deeply erosive contacts. These commonly orange, ochre and yellow-weathering, well-cemented, massive coquinas contain between 60% and 95% shells, including gastropods (e.g. *Turritella* and *Chorus* sp.), *Chlamys* sp., venerids, bivalves, barnacles, oysters, as well as rare cetacean bones, within a calcareous or fine shell hash matrix. Locally small lenses of coquina are composed almost exclusively of articulated *Mulinia* cf. *vidali* (Philippi, 1887). Whole rosetted barnacles up to 20 cm in diameter are attached in life position to some shell hash surfaces. In Unit 3 of the Pachingo 3 section, the facies is composed almost entirely of unoriented whole *Turritella* shells within a calcareous sandy matrix (Fig. 8). The *Turritella* sp. is very similar to *Turritella breantiana* of other authors (Philippi, 1887; Tavera, 1979), which is a replacement name for *Turritella monilifera* (Forbes, 1846), a Late Cretaceous species from India. Philippi (1887) gave it the name *Turritella leptogramma*, which is the correct designation.

At Pachingo 3, this facies fills a 2-m-deep, 20-m-wide, asymmetric channel cut into Unit 5. The channel-fill is a fine to medium calcareous sandstone containing articulated oysters, pectens, barnacles and some gastropods, as well as shell fragments and rounded to sub-rounded pebbles and cobbles of andesite, chert, sandstone, and phosphate concentrated near the steep edge of the channel. The top of the unit comprises a fine, faintly cross-stratified coquina of fragmented and whole barnacles, some of which form clusters around cobbles. Herm (1969) noted that some pebbles served as settling points for *Crepidula*. The channel-fill deposits clearly fine upwards.

In the type section at Pachingo 3, the coquinas are interbedded with sandy, less shelly horizons a few cm thick and spaced up to 40 cm apart, showing horizontal and low-angle planar cross-stratification. In the Tongoy 2 section, between the coquina beds and in some cases grading downward into them, are medium to fine sandstones with occasional *Thalassinoides* burrows and fish scales. At Almendros 2.2, the coquinas are interbedded with grey, yellow and ochre-weathering, fine to medium sandstones containing 10 to 30% shell fragments, of which 95% are barnacles. Oyster fragments as well as

Fig. 8. *Turritella leptogramma* shells in facies 3, Unit 1 (Pachingo 3).

scattered pebbles are also present. In Pachingo 2, three coquina beds fine upward into greenish to yellowish very fine sandstone.

In some localities, facies 3 grades laterally and/or vertically into facies 2, indicating that they were deposited under similar conditions. In Unit 15 of the Pachingo 3 type section, for example, calcareous conglomerate with subrounded to rounded sandstone and andesite pebbles are interbedded with and grade into coquina with *Turritella*, *Acanthina unicornis* (Bruguière, 1789), barnacles, bivalves, and scattered small pebbles, as well as fine to medium, calcareous sandstones with gastropods, bivalves and limestone clasts. In Almendros 2.2, a pebbly coquina with up to 20% rounded clasts, dominated by barnacles but also containing oysters and gastropods, is overlain by a coquina with 80–95% shell fragments and scattered pebbles. Some sandstone lenses as well as cetacean bones are also present.

5.3.2. Interpretation

The coquinas are interpreted as nearshore (upper shoreface) deposits because of their high fossil content, including *Balanus* in life position, as well as *Ostrea* and *Turritella* sp. The fact that these macrofossils are mostly preserved whole, suggests local assemblages with little subsequent reworking. A high-energy nearshore environment is confirmed by the robust, thick-shelled bivalves *Mulinia* cf. *vidali*. According to Bourgeois and Leithold (1984) such thick-shelled species is one of the most diagnostic criteria for shallow marine environments. *Thalassinoides* burrows are reported by MacEachern and Hobbs (2004) in conglomeratic sandstones of bay margin deposits in Alberta and British Columbia.

Where the coquinas form lenses of unoriented *Turritella* and other shallow marine shells overlying sharp, planar contacts, they probably represent offshore bars or shoals subjected to variable currents and wave action. The presence of low-angle cross-lamination may indicate local beach development on shoals partially emergent during low spring tides (Clifton, 1969; Tucker and Wright, 1990). Deeply eroded scours filled with coquina, on the other hand, are interpreted as tidal channels, rip-current channels formed during storms, or even the underwater extensions of fluvial channels (Gruszczynski et al., 1993). High current velocities are indicated by upper flow regime plane laminae as well as cobbles up to 20 cm in diameter. Similar scours are common in the upper shoreface environment, as described for example from Miocene sandstones at Floras Lake, Oregon (Bourgeois and Leithold, 1984). Here, the scours are commonly asymmetric, with one wall close to vertical and the other inclined at 30° to 45°, as in Pachingo 3. They are filled with gravel and shell fragments occurring within medium to coarse sandstones, with a concentration of larger clasts against the steep wall. This, together with the crudely fining-upward nature of the fill, as at Pachingo 3, was interpreted by Bourgeois and Leithold (1984) as indicative of unidirectional currents with waning flow.

Facies similar to those described above have also been interpreted by Carter and Naish (1998) as upper shoreface deposits. In the Tongoy paleobay, this facies represents shelly shoals and channels, but more distant from the river mouths than facies 2. Local pebble concentrations indicate the sporadic influx of continental material during peak river discharge periods, redistributed by waves and marine currents during storms.

5.4. Facies 4: multicoloured, swaley and trough cross-stratified, coarse- to fine-grained sandstones, siltstones and shales

5.4.1. Description

This facies composes Units 7, 9, and 16. It consists of purplish to brownish, coarse to fine, clay-rich sandstones showing occasional trough and swaley cross-stratification. Although exposed in cliff sections where it is difficult to measure the exact orientation of the troughs, they generally trend parallel to the nearest inferred shoreline. Some fining-upward units, 100 to 250 cm thick, consist of sandstones grading upward into varicoloured siltstones, clay or shale. Bed thicknesses are generally less than 30 cm. Some siltstone beds contain up to 10% whole gastropods, as well as up to 5% well-rounded pebbles reaching 3 cm in diameter. Locally, for example, in Unit 16 of the Pachingo 3 section, the sandstones are interbedded with white nodular limestone beds and lenses containing barnacles and scattered pebbles. Herm (1969) mentioned some dense venerid populations in this facies. Some bioturbation is also present, with *Skolithos* identified in a grey to ochre-weathering, fine to medium, laminated sandstone in the Almendros 1 section.

5.4.2. Interpretation

The overall grain size of this facies is between that of facies 3 and 5, suggesting a transitional environment. This is supported by the presence of barnacles and pebbles in the interbedded limestones, which indicate that the shoreline was not too far away (Carter and Naish, 1998). The shore-parallel trend of trough cross-lamination in the sandstones possibly indicates the migration of lunate dunes along incipient runnel

systems, whereas the presence of swales suggests occasional high-energy, stormy conditions disturbing the ocean floor. This is also implied by the occurrence of *Skolithos*. These beds are therefore interpreted as middle shoreface deposits.

5.5. Facies 5: multicoloured, massive, fine-grained sandstones, siltstones and laminated shales with diatomaceous clay lenses

5.5.1. Description

Facies 5 only occurs in Unit 5. At Pachingo 3, it consists of pale green fine sandstone with rare lenses and beds of white, diatomaceous, laminated clay. The sandstone is massive with scattered fine shell fragments and is intensively bioturbated by very small, sinuous burrows referred to *Macaronichnus segregatus*. Some larger, oblique burrows are also present. At Pachingo 1 and Almendros 1, this facies is represented by a multicoloured succession of medium to fine sandstones, siltstones, and laminated shales.

5.5.2. Interpretation

The interbedded fine sandstones, siltstones and shales of this facies are typical of the lower shoreface environment (Galloway and Hobday, 1983; Le Roux and Jones, 1994; Le Roux and Elgueta, 1997). This is supported by the presence of *Macaronichnus segregatus*, which commonly occurs at the base of the shoreface zone (Clifton and Thompson, 1978; Hunter, 1980; Clifton, 1981; Leckie and Walker, 1982; Bergman, 1994). The presence of diatomaceous clay lenses also indicates a transitional environment with facies 6.

5.6. Facies 6: tuffaceous, diatomaceous, and microfossiliferous shales and clays with nodular phosphate beds

5.6.1. Description

This facies occurs in Units 4, 11 and 14. It is dominated by multicoloured, tuffaceous clay showing lower flow regime planar laminae and green to dark brown shales with diatoms and fish scales, as well as thin, very fragile but well-preserved bivalve and gastropod shells. The shales are locally interbedded with thin fine to medium sandstones and laminated diatomaceous clays. The latter are light brown to white-weathering, occurring as single horizons or interbedded with brown siltstone and greyish fine sandstone. These diatomaceous beds are rich in planktonic diatoms (about 70%) characteristic of a highly productive marine environment. About 88% of the diatoms comprise species of *Chaetoceros*, *Thalassionema* and *Thalassiothrix*. They occur together with cosmopolitan planktonic forms that include several *Coscinodiscus* species (Table 2). They also contain ebridians (2%), dinoflagellates (3%), silicoflagellates (5%) and radiolaria (López, 1965; Martínez and Caro, 1980), as well as rare siliceous sponge spicules.

Within this facies at Pachingo 3 is a 20-cm-thick bed of phosphate pebbles with an erosional basal contact (Fig. 9). The nodular clasts vary from a few mm to

Fig. 9. Phosphate pebble bed in facies 6, overlying erosional surface. The pebbles were probably derived from a phosphate hardground eroded and reworked during a major storm (Pachingo 3).

more than 20 cm in diameter, with some of the larger cobbles showing borings. The bed is enriched in bone fragments and shark teeth (*Cosmopolitodus hastalis*).

5.6.2. Interpretation

The very fine grain size of this unit, together with the presence of abundant diatoms, fish scales and whole delicate shells, suggest a low-energy, relatively deep-water environment. This is supported by the mm-scale lower flow regime horizontal lamination. The nodular, bored phosphate pebble bed in Pachingo 3 probably represents a phosphate hardground eroded during a storm that redistributed the clasts. According to the classification of Garrison and Kastner (1990), it is a type D-phosphate which normally forms as a consequence of extended periods of non-deposition and winnowing in the shelf and upper continental slope environment (Burnett et al., 1980; Garrison et al., 1987; Garrison, 1992). The latter, however, can be ruled out within a bay setting.

Martínez and Caro (1980) postulated a water depth between 25 and 30 m for these deposits because of the presence of *Actinoptychus senarius*, *Actinocyclus octonarius*, *Auliscus caelatus* and *Grammatophora angulosa*, which they considered to be characteristic of the infralittoral zone. However, they also pointed out that this is contradicted by the presence of other species such as *Actinocyclus ellipticus* and *Coscodiscus oculoiridis*, which are typical oceanic forms.

More recent information on the distribution of these supposedly shallow-water species does not support this hypothesis. *Actinoptychus senarius* is a typical neritic species, although it has also been reported from Neogene upper continental slope sediments in Chile (Le Roux et al., 2005b), where it occurs together with *Paralia sulcata*, as well as *Grammatophora*, *Coscinodiscus*, *Diploneis* and *Rhaponeis* spp. *Actinocyclus octonarius* in fact prefers open water, although it has been found in brackish-marine environments (Sohlenius et al., 1996). More specifically, both *Actinoptychus senarius* and *Actinocyclus octonarius* have been found in sediments in the middle of Chesapeake Bay (L.M. Weimer, unpublished report on Internet site http://pubs.gov/pdf/of/of99-45/diatom.pdf). *Grammotophora angulosa* has also been reported from the Bay of Fundy, where it occurs in water depths up to 200 m (Internet site http://gmbis.marinebiodiversity.ca/BayOfFundy/taxListInfo.jsp?taxListInfo=Grammatophora%20angulosa).

Facies 6 is therefore considered to represent inner bay sediments in relatively deep water (100–140 m).

5.7. Facies 7: multicoloured fine to very fine, microfossiliferous sandstones with thin coquina beds, grading upward into mudrocks

5.7.1. Description

This facies is characterized by multicoloured, repetitive fining-upward successions of fine to very fine clay-rich, bioturbated sandstones capped by clay and mudstone intervals up to 6 m thick. The sandstones are generally massive with rare ripple cross-lamination and upper flow regime planar lamination. The thickness of individual beds or fining-upward units varies from 30 cm to 7 m. Scattered macrofossils are represented by whole *Chorus* sp., *Chlamys hupeanus*, molds of unidentified bivalves, cetacean bones, fish scales and teeth of the great white shark *Carcharodon carcharias*. *Skolithos* and *Ophiomorpha* burrows filled with medium sand are preserved in places.

López (1965) reported that samples from the Coquimbo Formation were mostly barren of foraminifers, as was confirmed by our own studies. From this facies near the top of Unit 11, however, she recovered a large variety of foraminifers including *Globigerina bulloides*, *Textularia secasensis*, *Buccella meridionalis*, *Planula wuellerstorfi*, *Cassidulina laevigata* var. *carinata*, *Virgulina compressa*, *Angulogerina angulosa*, *Hanzawaia schmitti*, *Nonionella auris* var. *stella*, *Bolivina striatula*, *Buliminella elegantissima*, and *Dyocibicides biseriales*. Foraminifers from the top of Unit 14 include *Globigerina bulloides* and unidentified *Buccella* sp.

Thin fossiliferous interbeds contain fragmented and articulated pectens, oysters, barnacles, bivalves, and gastropods including *Turritella*, together with small, scattered pebbles (Fig. 10). The matrix is composed of shell hash that fines upward from sharp basal contacts.

5.7.2. Interpretation

The fine, massive, bioturbated sands were probably deposited in relatively deep water, interpreted here as an inner shelf/bay environment. This is indicated by the generally fine grain size of the deposits and the presence of typical deeper water benthonic foraminifers. *Crassidulina laevigata*, for example, has been collected from a depth below 95 m on the Guadiana Shelf (Mendes et al., 2004) and also occurs on the northern Iceland Shelf (Jennings et al., 2004). *Nonionella auris* occurs preferentially in low energy, deep environments with muddy substrates within the San Matias Gulf of Argentina (Bernasconi and Cusminsky, 2005). *Globigerina bulloides* lives above the thermocline at water

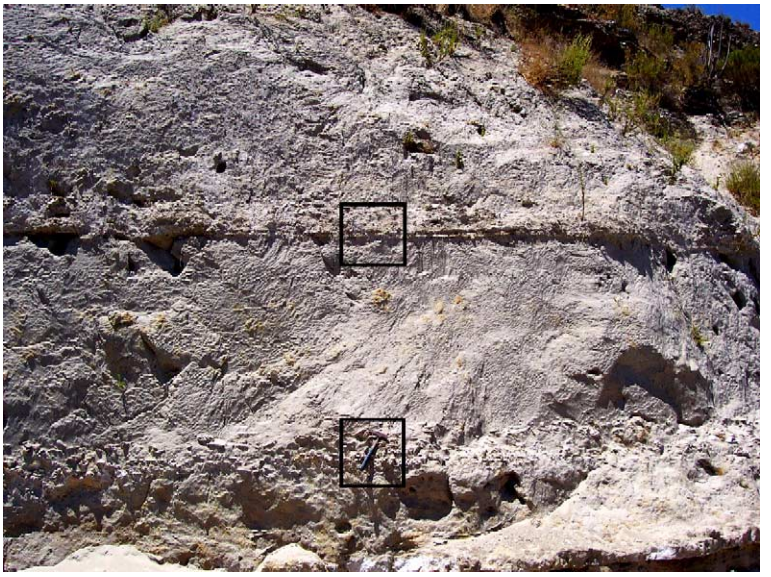

Fig. 10. Massive, bioturbated sandstone and tempestites (thin shelly beds at rectangles) of facies 7 in Unit 11 (Tongoy 2). Hammer (within lower rectangle) for scale.

depths below 50 m (Fairbanks et al., 1982) and is also abundant on the inner shelf (Phleger, 1960). The presence of *Angulogerina angulosa* and *Buliminella elegantissima* suggests water depths between 135 and 150 m (Ingle et al., 1980).

The repetitive, fining-upward nature of the beds indicates that they may have been produced by turbidity currents, with flow structures subsequently destroyed by bioturbation. This could explain the occurrence of shallow water species such as *Chlamys*, which may have been transported from nearshore zones. Such density currents may have been the result of sporadic rainfall events in the mountainous terrain flanking the paleobay, flooding the rivers and discharging fine sand and silt into the bay in addition to gravels near the shoreline.

Both *Ophiomorpha* and *Skolithos* are associated with environments characterized by frequent high-energy events, drastic changes in the sedimentation rate and erosion of surface sediments (Walker and James, 1992).

The thin fossiliferous interbeds overlying sharp contacts are interpreted as tempestites, as suggested by their erosive bases and fining-upward nature, as well as the presence of nearshore species such as *Balanus*, *Ostrea* and *Chlamys*, which can be attributed to redistribution into deeper water by these events (Walker and James, 1992).

6. Relative sea-level changes

The stratigraphic distribution of the facies described above (Table 1) allows reconstruction of relative sea-level changes in the Tongoy paleobay during the Neocene.

The exposed succession starts with the deposition of *Turritella* coquinas in an upper shoreface environment (20 m depth), some time before 12 Ma. A relative marine regression subsequently allowed the development of a subaerial karst surface and terra rossa soil profile, which was inundated by marine transgression to a depth of about 15 m shortly before 11.9 Ma. This transgression lasted until about 11.2 Ma and inundated the bay to depths of about 120 m. A relative regression from 11.2 to 10.1 Ma to estuarine/upper shoreface depths (15 m) was followed by minor transgression lasting until 9.5 Ma and reaching middle shoreface depths (50 m). A regression culminating at 9.0 Ma established fluvio-estuarine conditions with the deposition of coarse gravels during peak run-off periods. From 9.0 to 7.3 Ma, renewed transgression led to depths of 40 m in the bay, followed by another regression to fluvio-estuarine conditions at 6.3 Ma. At 5.3 Ma, a major transgression to 100 m depths is recorded. Regression to fluvio-estuarine depths peaked at 4.3 Ma, followed by another major transgression to 100 m depths by 2.2 Ma. Renewed submergence to estuarine/upper shoreface conditions occurred up to 1.7 Ma, followed by transgression to 50 m depths at about 1.4 Ma. At 0.3 Ma, a marine terrace (Talinay IV) was eroded at the top of the stratigraphic section at Pachingo 3. After three more sea-level oscillations during the Quaternary, this surface was uplifted to about 105 m a.s.l.

7. Discussion

Le Roux et al. (2005a) modelled the regional tectonic behaviour of the crust at Tongoy using geohistory analysis (Van Hinte, 1978). This involves determining the age and depth of deposition of each stratigraphic unit, relating this depth to contemporaneous eustatic sea level using published sea level curves, and calculating the relative elevation of a reference surface (in this case, the base of the measured column at Pachingo 3) through time. Le Roux et al. (2005a) concluded that crustal subsidence of at least 75 m occurred between 11.9 and 10.5 Ma, followed by uplift of about 55 m at 0.02 mm/year associated with the approach and subduction of the NE-striking branch of JFR from the north (Figs. 1 and 11). The relative rate of convergence between the Nazca and South American plates was calculated at 6.2 cm/year during the time of subsidence, which accelerated to 10.1 cm/year from 7.7 to 6.9 Ma, when crustal uplift ended. Renewed subsidence in the wake of the southward-migrating JFR took place at a rate of 0.02 mm/year and totalled about 110 m, which was followed by rapid uplift of ca. 175 m at a rate of 0.08 mm/year after 2.1 Ma. The last event was attributed by Le Roux et al. (2005a) to the subduction of an oceanic plateau similar to the JFR, but with a strike of 014° instead of 030°, at this locality.

These relatively slow rates of uplift and subsidence reflect the regional tectonic effects of the JFR and associated oceanic plateaus, but do not represent short-period, local tectonics caused by faulting. Table 3 shows that a relatively strong subsidence episode of −0.07 mm/year took place between 10.1 and 9.5 Ma, during the period of general uplift between 10.5 and 6.9 Ma, while a very rapid uplift event of 0.34 mm/year occurred between 5.3 and 5.0 Ma, during the period of general subsidence between 6.9 and 2.1 Ma. These opposite tectonic movements may be related mainly to the eastward-dipping Puerto Aldea Fault along the western limit of the study area (Figs. 2 and 3). Field studies indicate that it is essentially a normal fault, as proposed by Herm et al. (1967) and confirmed by Paskoff (1970) and Martínez (1979).

Heinze (2003) collected numerous fault–slip data along secondary fault planes of the Puerto Aldea Fault. Vertical offsets ranged from 0.1 to 5.2 m, with the dip direction varying between WSW and ENE (average = 084°) at a dip angle of 60° to 80° (average = 64°). Multiple slickensides on identical slip surfaces indicate that about 30% of all fault planes underwent multiple stages of deformation, with the predominant deformation being due to oblique dip–slip motion (~55%) towards 048°, followed by strike–slip (~35%) at 158° and reverse slip (~10%) towards 175°. Heinze (2003) concluded that trench-parallel faults within the basin are still subject to deformation processes, with elastic dislocation modelling indicating that deformation along them is associated with co-seismic rupture at crustal depth (10–20 km).

Within the Coquimbo beds, we observed small-scale eastward-dipping, step-like normal displacements that may have been formed during reactivation of the Puerto Aldea Fault. However, there are also indications of reverse movement along this contact. Just south of Puerto Aldea, the Coquimbo beds steepen to a 30° westward dip from an almost horizontal attitude less

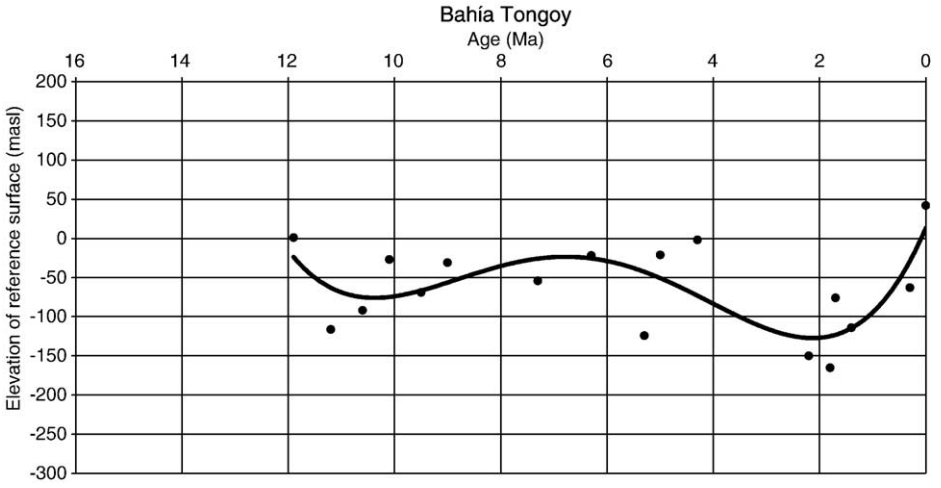

Fig. 11. Tectonic behaviour of the crust as derived from geohistory analysis. The uplift commencing at 10.5 Ma is related to the approach of the Juan Fernández Ridge, followed by subsidence in its wake from 6.9 to 2.1 Ma.

Table 3
Relationship between global and relative sea levels at the Bay of Tongoy (locality Pachingo 3) during the Miocene–Pleistocene, with deduced tectonic elevations

Unit	Age (Ma)	Error in ages		Cumulative thickness (m)	Global sea level (m)	Depth of depositional interface (m)	Elevation of reference contact (m)	Rate of change (mm/year)
		A	B					
Final uplift			0	63	0	105	42	+0.35
Talinay IV	0.3			63	0 ± 3	0	−63 ± 3	+0.06
16 (middle)	**1.4**	±0.1	±0.4	63	−1 ± 25	−50 ± 20	−114 ± 45	−0.13
15 (middle)	**1.7**	±0.1	±0.4	58	−3 ± 24	−15 ± 20	−76 ± 45	+0.76
14 (top)	**1.8**	±0.1	±0.4	56	−9 ± 26	−100 ± 40	−165 ± 66	−0.04
14 (middle)	**2.2**	±0.1	±0.4	49	−1 ± 27	−100 ± 40	−150 ± 67	−0.07
13 (middle)	4.3			40	48 ± 28	−10 ± 5	−2 ± 33	+0.03
12 (base)	**5.0**	±0.1	±0.6	39	38 ± 37	−20 ± 20	−21 ± 57	+0.34
11(base)	**5.3**	±0.1	±0.6	33	9 ± 7	−100 ± 40	−124 ± 47	−0.10
10 (middle)	6.3			30	18 ± 18	−10 ± 5	−22 ± 23	+0.02
9 (middle)	7.3			27	23 ± 6	−50 ± 20	−54 ± 26	−0.01
8 (middle)	**9.0**	±0.4	±0.6	22	1 ± 17	−10 ± 5	−31 ± 22	+0.08
7 (middle)	9.5			18	−1 ± 17	−50 ± 20	−69 ± 37	−0.07
6 (middle)	10.1			13	1 ± 18	−15 ± 20	−27 ± 38	+0.13
5 (middle)	10.6			9	−3 ± 24	−80 ± 20	−92 ± 44	+0.04
4 (middle)	11.2			4	8 ± 33	−120 ± 20	−116 ± 53	−0.17
3 (middle)	**11.9**	±0.3	±0.7	2	18 ± 43	−15 ± 20	1 ± 63	

Ages in bold print were obtained from direct Sr-dating.
Uncertainty in ages due to (A) measurement of Sr isotopic ratios (relative error) and (B) uncertainty in the Tertiary seawater evolution curve (absolute error) of McArthur et al. (2001). Error in measurement of Sr ratio assuming ±0.0020%, 95% confidence limit.

than 50 m from the faulted contact. In this area are small-scale, steeply eastward-dipping normal displacements within the Coquimbo Formation, some of which also show reverse movement (Fig. 12). Lithologically, these beds are very similar to Unit 11, although no definite correlation is possible because of incomplete exposure of the Coquimbo Formation at this locality.

A possible explanation for these movements along the Puerto Aldea Fault during regional uplift and downwarp events is shown in Fig. 13. The shape of the as yet unsubducted part of the JFR west of the continent is shown by bathymetric contours and profiles to have higher slopes closer to the ridge crest (Morales, 1984). Regional uplift produced by the JFR wedging in be-

Fig. 12. Steeply westward-dipping beds of the Coquimbo Formation. Note small-scale, eastward-dipping reverse displacement in Coquimbo beds (within rectangle, which also contains hammer in lower left-hand corner for scale).

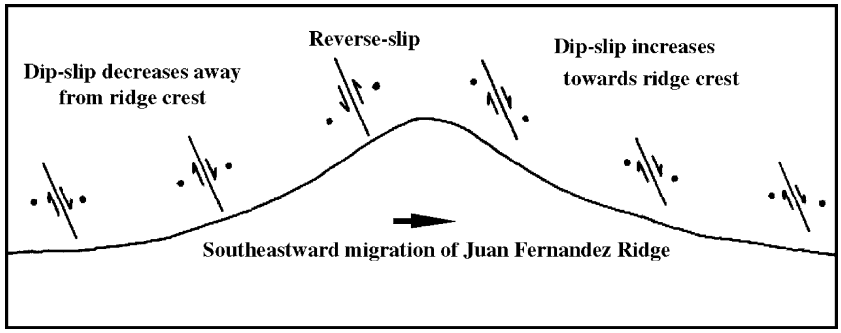

Fig. 13. Explanation of opposite tectonic movements produced along the Puerto Aldea Fault by the southeastward-migrating JFR. Black dots are at equal distances from the ridge surface and are increasingly displaced vertically relative to each other during the approach of the JFR crest, causing downfaulting to the southeast. In the wake of the JFR, vertical stresses are reversed, being highest just to the northwest of the ridge crest and causing reverse movement along the fault. This reverts again to normal displacement as the crest moves away.

neath this part of the crust would therefore have caused strong, upward-directed stress in the area close to the ridge, i.e. just to the southeast thereof, whereas the area farther to the southeast would have been subjected to weaker vertical stresses (compare black dots in Fig. 13). The resultant differential stress field across this zone would have caused downfaulting to the east, reactivating the Puerto Aldea Fault in the normal sense. Local pulses of subsidence because of normal faulting would therefore have been superimposed on the regional uplift caused by the approaching JFR. This would have been especially prominent just before the arrival of the crest below this part of the crust, as also indicated by the 9.0–7.3 Ma event. As the JFR migrated past this area, however, subsidence in its wake would have had the opposite effect just northwest of the ridge crest, where the largest vertical stresses would have operated. This would have caused pulses of reverse movement along the Aldea Fault and short uplift events superimposed on the regional downwarp. The uplift event starting at 5.3 Ma occurred relatively soon after the ridge crest had passed this locality at 6.9 Ma. There is a somewhat longer delay in fault reactivation as compared to the first downwarp event that ended at 7.3 Ma, which occurred within 0.4 Ma before the arrival of the crest, but this can probably be attributed to the high fault angle, which would have been more resistant to reverse movement than to normal displacement. As the JFR migrated further southeast, the initial reverse movement along the fault would have reverted again to normal faulting (Fig. 13), so that the period of reverse movement would have been relatively short. This confirms the correlation of the beds in Fig. 12 with Unit 11, which has an age of around 5.3 Ma and would have experienced reverse faulting only during this period when the area was close to the ridge crest. If these beds were younger, they would have been subjected only to normal stresses as the JFR crest migrated further southeast. The absence of breccia in the Coquimbo beds along the Puerto Aldea Fault, compared to the highly brecciated nature of the basement, suggests that Unit 11 was relatively unconsolidated at the time and experienced synsedimentary faulting.

The rather abrupt changes in water depths recorded in the Coquimbo Formation can thus be attributed to the effect of local tectonics, with downfaulting causing rapid transgression and reverse faulting leading to regression.

8. Conclusions

Bay sedimentation at Tongoy was strongly influenced by relative sea level fluctuations caused by eustatic changes and both regional and local tectonic controls. During marine transgressions, water depths increased to a maximum of about 120 m, with the deposition of diatomaceous mudstones, siltstones and fine sandstones intercalated with occasional shelly storm beds. Regressions led to upper shoreface conditions with pebbly shell beds deposited in tidal channels and on shoals. During periods of high rainfall in the fluvial drainage basins, coarse gravelly sediments were transported into the bay and mixed with shells of nearshore fauna.

Subduction of the Juan Fernández Ridge caused a slow elevation of the area (0.02 mm/year) from 10.5 to 6.9 Ma, followed by equally slow subsidence as the ridge migrated southeastward. However, opposite tectonic movements with much higher rates of uplift or subsidence were produced along the Aldea Fault as a result of differential stress fields across the JFR. Strong uplift commencing at 2.1 Ma, possibly related to the subduction of an oceanic plateau similar to the JFR, finally elevated the bay above sea level.

The combination of tectonic movements with eustatic sea-level changes is the main cause of the very rapid lateral and vertical facies changes observed within the bay deposits of the Coquimbo Formation, overshadowing the effects of natural coastal progradation or erosion.

Acknowledgements

We appreciate the very thorough and critical reviews of two anonymous reviewers, as well as editor Keith Crook. This project was funded by Fondecyt 1010691, which is gratefully acknowledged. Mario Suárez of the Palaeontological Museum in Caldera kindly identified the shark teeth in the Coquimbo Formation. SNN acknowledges support by grant NI 699/4-1 of the Deutsche Forschungsgemeinschaft (DFG).

References

Alpers, C.N., Brimhall, G.H., 1988. Middle Miocene climatic change in the Atacama Desert, northern Chile: evidence from supergene mineralization at La Escondida. GSA Bulletin 100, 1640–1656.

Arnott, R.W.C., 2003. The role of fluid- and sediment-gravity flow processes during deposition of deltaic conglomerates (Cardium Formation, Upper Cretaceous), west-central Alberta. Bulletin of Canadian Petroleum Geology 51, 426–436.

Benado, D.E., 2000. Estructuras y Estratigrafıa Básica de Terrazas Marinas en Sector Costero de Altos de Talinay y Bahía Tongoy: Implicancia Neotectónica. Memoria, Universidad de Chile.78 pp.

Bergman, K.M., 1994. Shannon Sandstone in Hartzog Draw: Heldt Draw Fields (Cretaceous, Wyoming, USA) reinterpreted as lowstand shoreface deposits. Journal of Sedimentary Research B64, 184–201.

Bernasconi, E., Cusminsky, G., 2005. Distribution of *Nonionella auris* (d'Orbigny) (Foraminiferida) in San Matias Gulf, Rio Negro Province, Argentina. Ameghiniana 42, 167–174.

Bourgeois, J., Leithold, E.L., 1984. Wave-reworked conglomerates — depositional processes and criteria for recognition. In: Koster, E.H., Steel, R.J. (Eds.), Sedimentology of Gravels and Conglomerates. Canadian Society of Petroleum Geologists, Calgary, pp. 331–343.

Brüggen, J., 1950. Fundamentos de la Geologıa de Chile. Instituto Geográfico Militar, Santiago. 374 pp.

Bruguière, J.G., 1789. Encyclopédie Méthodique. Histoire Naturelle des Vers, vol. 1. Panckoucke, Paris. 344 pp.

Burnett, W.C., Veeh, H.H., Soutar, A., 1980. U-series, oceanographic and sedimentary evidence in support of recent formation of phosphate nodules. In: Bentor, Y.K. (Ed.), Marine Phosphates — Geochemistry, Occurrence, Genesis. Society of Economic Paleontologists and Mineralogists, Spec. Publ., vol. 29, pp. 61–71.

Carter, R.M., Naish, T.R., 1998. A review of Wanganui Basin, New Zealand: global reference section for shallow marine, Plio-Pleistocene (2.5–0 Ma) cyclostratigraphy. Sedimentary Geology 122, 37–52.

Clifton, H.E., 1969. Beach lamination: nature and origin. Marine Geology 7, 553–559.

Clifton, H.E., 1973. Pebble segregation and bed lenticularity in wave-reworked versus alluvial gravel. Sedimentary Geology 20, 173–187.

Clifton, H.E., 1981. Progradational sequences in Miocene shoreline deposits, southeastern Caliente Range, California. Journal of Sedimentary Petrology 51, 165–184.

Clifton, H.E., Thompson, J.K., 1978. *Macaronichnus segregatus*: a feeding structure of shallow marine polychaetes. Journal of Sedimentary Petrology 48, 1293–1302.

Dalrymple, R.W., Zaitlin, B.A., Boyd, R., 1992. Estuarine facies models: conceptual basis and stratigraphic implications. Journal of Sedimentary Petrology 62, 1130–1146.

De Muizón, C., DeVries, T., 1985. Geology and paleontology of Late Cenozoic marine deposits in the Sacaco area (Peru). Geologische Rundschau 74, 547–563.

DeVries, T.J., 2003. *Acanthina* Fischer von Waldheim, 1807 (Gastropoda: Muricidae), an ocenebrine genus endemic to South America. Veliger 46, 332–350.

DeVries, T.J., in press. Cenozoic Turritellidae (Gastropoda) from southern Peru. Journal of Paleontology.

Dunbar, R.B., Marty, R.C., Baker, P.A., 1990. Cenozoic marine sedimentation in the Sechura and Pisco basins. Palaeogeography, Palaeoclimatology, Palaeoecology 77, 235–261.

Esteban, M., Klappa, C.F., 1983. Subaerial exposure environment. In: Scholle, P.A., Bebout, D.G., Moore, C.H. (Eds.), Carbonate Depositional Environments, Memoir of the American Association of Petroleum Geologists, vol. 33, pp. 1–54.

Fairbanks, R.G., Sverdlove, M., Free, R., Wiebe, P.H., Bé, W.H., 1982. Vertical distribution and isotopic fractionation of living foraminifera from the Panama Basin. Nature 298, 841–844.

Finger, K., Encinas, A., Nielsen, S., Peterson, D., 2003. Microfaunal indications of late Miocene deep-water basins off the central coast of Chile. 10° Congreso Geológico Chileno, Concepción, Chile. Abstract Volume CD-ROM. 8 pp.

Flower, B.P., Kennett, J.P., 1993. Middle Miocene ocean–climate transition: high-resolution oxygen and carbon isotopic records from Deep Sea Drilling Project Site 588A, southwest Pacific. Paleoceanography 8, 811–843.

Forbes, F., 1846. Report on the fossil Invertebrata from South India. Transactions of the Geological Society of London 7, 97–174.

Galloway, W.E., Hobday, D.K., 1983. Terrigenous Clastic Depositional Systems. Applications to Petroleum, Coal and Uranium Exploration. Springer-Verlag, New York.

Gana, P., 1991. Mapa Geológico de la Cordillera de la Costa entre La Serena y Quebrada El Teniente, Región de Coquimbo. Escala 1:100000. Documento de Trabajo No. 3, SERNAGEOMIN, Santiago, Chile.

Garrison, R.E., 1992. Neogene phosphogenesis along the eastern margin of the Pacific Ocean. Revista Geológica de Chile 19, 91–111.

Garrison, R.E., Kastner, M., 1990. Phosphatic sediments and rocks recovered from the Peru margin during ODP Leg 112. In: Suess, E. (Ed.), Proceedings of the Ocean Drilling Program, Peru Continental Margin, Leg 112. College Station, Scientific Results, Texas, pp. 111–134.

Garrison, R.E., Kastner, M., Kolodny, Y., 1987. Phosphorites and phosphatic rocks in the Monterey Formation and related Miocene units, coastal California. In: Ingersol, R.V., Ernst, W.D. (Eds.), Prentice Hall, Englewood Cliffs, NJ, pp. 349–381.

Gregory-Wodzicki, K.M., 2000. Uplift history of the Central and Northern Andes: a review. GSA Bulletin 112, 1091–1105.

Gruszczynski, M., Rudowski, S., Semil, J., Slominski, J., Zrobek, J., 1993. Rip currents as a geological tool. Sedimentology 40, 217–236.

Guzmán, N., Marquardt, C., Ortlieb, L., Frassinetti, D., 2000. La malacafauna neógena del área de Caldera (27°–28°S): especies y rangos bioestratigráficos. Abstracts, IX Congreso Chileno, Puerto Varas, vol. 1, pp. 476–481.

Heinze, B., 2003. Active intraplate faulting in the forearc of north central Chile (30°–31°S): implications from neotectonic field studies, GPS data, and elastic dislocation modelling. Scientific Technical Report - Geoforschungszentrum Potsdam 03/07. 127 pp.

Herm, D., 1969. Marines Pliozän und Pleistozän in nord- und mittel-Chile unter besonderer Berücksichtigung der Entwicklung der Mollusken-Faunen. Zitteliana 2, 1–159.

Herm, D., Paskoff, R., 1967. Vorschlag zur Gliederung des marinen Quartärs in Nord- und Mittel-Chile. Neues Jahrbuch für Geologie und Paläontologie. Monatshefte 10, 577–588.

Herm, D., Paskoff, R., Stiefel, J., 1967. Première observations sur les alentours de la baie de Tongoy (Chili). Bulletin de la Société Géologique de France 7 série (8), 21–24.

Hinojosa, L.F., 2005. Cambios climáticos y vegetacionales inferidos a partir de paleofloras cenozoicas del sur de Sudamérica. Revista Geológica de Chile 32, 95–114.

Hinojosa, L.F., Villagrán, C., 1997. Historia de los bosques del sur de Sudamérica: I. Antecedentes paleobotánicos, geológicos y climáticos del Terciario del cono sur de América. Revista Chilena de Historia Natural 70, 225–239.

Hunter, R.E., 1980. Depositional environments of some Pleistocene coastal terrace deposits, southwestern Oregon — case history of a progradational beach and dune sequence. Sedimentary Geology 27, 241–262.

Ingle, J., Keller, G., Kolpack, R., 1980. Benthic foraminiferal biofacies, sediments and water masses of the southern Peru–Chile Trench area, southern Pacific Ocean. Micropaleontology 26, 113–150.

International Commission on Stratigraphy, 2004. International Stratigraphic Chart.

Jennings, A.E., Weiner, N.J., Helgadottir, G., Andrews, J.T., 2004. Modern foraminiferal faunas of the southwestern to northern Iceland shelf: oceanographic and environmental controls. Journal of Foraminiferal Research 34, 180–207.

Kumar, N., Sanders, J.E., 1976. Characteristics of shoreface storm deposits: modern and ancient examples. Journal of Sedimentary Petrology 46, 145–162.

Leckie, D.A., Walker, R.G., 1982. Storm- and tide-dominated shorelines in Cretaceous Moosebar–Lower Gates interval — outcrop equivalents of deep-basin gas traps in western Canada. American Association of Petroleum Geologists Bulletin 65, 138–157.

Leeder, M., 1999. Sedimentology and Sedimentary Basins: From Turbulence to Tectonics. Blackwell Science, Oxford. 592 pp.

Le Roux, J.P., Elgueta, S., 1997. Paralic parasequences associated with Eocene sea-level oscillations in an active margin setting: Trihueco Formation of the Arauco Basin, Chile. Sedimentary Geology 110, 257–276.

Le Roux, J.P., Elgueta, S., 2000. Sedimentologic development of a late Oligocene–Miocene forearc embayment. Valdivia Basin Complex, southern Chile. Sedimentary Geology 130, 27–44.

Le Roux, J.P., Jones, B.G., 1994. Lithostratigraphy and depositional environments of the Permian Nowra Sandstone in the southwestern Sydney basin, Australia. Australian Journal of Earth Sciences 41, 191–203.

Le Roux, J.P., Gómez, C., Fenner, J., Middleton, H., 2004. Sedimentological processes in a scarp-controlled rocky shoreline to upper continental slope environment, as revealed by unusual sedimentary features in the Neogene Coquimbo Formation, north-central Chile. Sedimentary Geology 165, 67–92.

Le Roux, J.P., Gómez, C.A., Olivares, D.M., Middleton, H., 2005a. Determining the Neogene behavior of the Nazca plate by geohistory analysis. Geology 33, 165–168.

Le Roux, J.P., Gómez, C., Venegas, C., Fenner, J., Middleton, H., Marchant, M., Buchbinder, B., Frassinetti, D., Marquardt, C., Gregory-Wodzicki, K.M., Lavenu, A., 2005b. Neogene–Quaternary coastal and offshore sedimentation in north-central Chile: record of sea level changes and implications for Andean tectonism. Journal of South American Earth Sciences 19, 83–98.

López, M.C., 1965. Estudio de los depósitos marinos de la Bahía de Tongoy. Memoria de Título. Departamento de Geologıa, Universidad de Chile, Santiago. 193 pp.

MacEachern, J.A., Hobbs, T.W., 2004. The ichnological expression of marine and marginal marine conglomerates and conglomeratic intervals, Cretaceous Western Interior Seaway, Alberta and northeastern British Columbia. Bulletin of Canadian Petroleum Geology 52, 77–102.

Martínez, R., 1979. Hallazgo de foraminıferos miocénicos cerca de Puerto Aldea, Bahía de Tongoy, Provincia de Coquimbo, Chile. Revista Geológica de Chile 8, 65–78.

Martínez, R., Caro, R., 1980. Micofósiles siliceos de las diatomitas de Tongoy, Provincia de Coquimbo, Chile: su significado biocronoestratigráfico, biocronológico, paleoecológico y paleogeográfico. Revista Geológica de Chile 10, 33–53.

McArthur, J.M., Howart, R.J., Bail, T.R., 2001. Strontium isotope stratigraphy: LOWESS Version 3: best fit to the marine Sr-isotope curve for 0–509 Ma and accompanying look-up table for deriving numerical age. Journal of Geology 109, 155–170.

Mendes, I., González, R., Dias, J.M.A., Lobo, F., Martins, V., 2004. Factors influencing recent foraminifera distribution on the Guadiana Shelf (southwestern Iberia). Marine Micropaleontology 51, 171–192.

Morales, E., 1984. Geografía de los Fondos Marinos del Mar Chileno. Instituto Geográfico Militar, Santiago. 206 pp.

Nemec, W., Steel, R.J., 1984. Alluvial and coastal conglomerates: their significant features and some comments on gravelly mass-flow deposits. In: Koster, E.H., Steel, R.J. (Eds.), Sedimentology of Gravels and Conglomerates. Canadian Society of Petroleum Geologists, Calgary, pp. 1–32.

Nichols, G., 1999. Sedimentology and Stratigraphy. Blackwell Science, Oxford. 355 pp.

Nielsen, S.N., DeVries, T.J., Encinas, A., Finger, K.L., Peterson, D. 2003. Towards an understanding of the age of the Navidad Formation. 10° Congreso Geológico Chileno, Concepción, Chile. Abstract Volume CD-ROM. 7 pp.

Pardo, M., Comte, D., Monfret, T., 2002. Seismotectonic and stress distribution in the central Chile subduction zone. Journal of South American Earth Sciences 15, 11–22.

Paskoff, R., 1970. Le Chili Semi-aride Recherches Géomorphologiques. Biscaye, Bordeaux. 420 pp.

Philippi, R.A., 1887. Die Tertiären und Quartären Versteinerungen Chiles. F.A. Brockhaus, Leipzig. 266 pp.

Phleger, F.B., 1960. Ecology and Distribution of Recent Foraminifera. John Hopkins Press, Baltimore. 297 pp.

Sohlenius, G., Sternbeck, J., Anden, E., Westman, P., 1996. Holocene history of the Baltic Seas as recorded in a sediment core from the Gotland Deep. Marine Geology 134, 183–201.

Sohn, Y.K., 2000. Depositional processes of submarine debris flows in the Miocene fan deltas, Pohang Basin, SE Korea with special reference to flow transformation. Journal of Sedimentary Research 70, 491–503.

Suárez, M.E., Marquardt, C., 2003. Revisión preliminar de las faunas de peces elasmobranquios del Mesozoico y Cenozoico de Chile: su valor como indicadores cronoestratigráficos. 10° Congreso Geológico Chileno, Concepción.

Suárez, M.C., Marquardt, C., Lavenu, A., Marinovic, N., Wilke, H.G., 2003. Invertebrados marinos neógenos de la Formación Portada, II Región, Chile. 10° Congreso Geológico Chileno, Concepción.

Tavera, J., 1979. Estratigrafia y paleontologıa de la Formación Navidad, Provincia de Colchagua (Lat. 30°50′–34°S). Boletín del Museo Nacional de Historia Natural de Chile 36. 176 pp.

Tsuchi, R., 1997. Marine climatic responses to Neogene tectonics of the Pacific Ocean seaways. Tectonophysics 281, 113–124.

Tsuchi, R., Shuto, T., Takayama, T., Fujiyoshi, A., Koizumi, I., Ibaraki, M., Martínez-Pardo, R., 1988. Fundamental data on Cenozoic biostratigraphy of Chile. Reports of Andean Studies, Shizuhoka University, Special, vol. 2, pp. 71–95.

Tsuchi, R., Shuto, T., Takayama, T., Koizumi, I., Fujiyoshi, A., Ibaraki, M., Martínez-P., R., 1990. Fundamental data on Cenozoic biostratigraphy of Chile-Supplement. Reports of Andean Studies, Shizuhoka University, Spec. Publ., vol. 3, pp. 59–71.

Tucker, M.E., Wright, V.P., 1990. Carbonate Sedimentology. Blackwell Scientific Publications, Oxford. 482 pp.

United States Army Corps of Engineers, 2002. Coastal Engineering Manual. Website http://www.usace.army.mil/inet/usace-docs/eng-manuals/em1110-2-1100/PartII.htm.

Van Hinte, J.E., 1978. Geohistory analysis: application of micropaleontology in exploration geology. American Association of Petroleum Geologists Bulletin 62, 201–222.

Walker, R., James, N., 1992. Facies Models: Response to Sea Level Change. Geological Association of Canada. 407 pp.

Wright, J.D., 1998. Role of the Greenlandã Scotland Ridge in Neogene climate changes. In: Crowley, T.J., Burke, K. (Eds.), Tectonic Boundary Conditions for Climate Model Simulations, Oxford Monographs on Geology and Geophysics, vol. 39. Oxford University Press, Oxford, UK, pp. 192–211.

Yáñez, G., Cembrano, J., Pardo, M., Ranero, C., Selles, D., 2002. The Challenger–Juan Fernández–Maipo major tectonic transition of the Nazca–Andean subduction system at 33–34°S: geodynamic evidence and implications. Journal of South American Earth Sciences 15, 23–38.